J. Fluid Mech. (1998), *vol.* 363, *pp.* 1–23. Printed in the United Kingdom

Görtler vortices: a backward-in-time approach to the receptivity problem

By PAOLO LUCHINI[1] AND ALESSANDRO BOTTARO[2]†

[1] Dipartimento di Ingegneria Aerospaziale, Politecnico di Milano, Via Golgi 40, 20133 Milano, Italy

[2] École Polytechnique Fédérale de Lausanne, CH-1015 Lausanne, Switzerland

(Received 23 December 1996 and in revised form 23 December 1997)

A quantitative definition of the receptivity of the Görtler instability is given by the Green's functions that external disturbances must be scalarly multiplied by in order to yield the amplitude of the most amplified instability mode, defined sufficiently far downstream of the plate's leading edge. These Green's functions (one for each kind of external disturbance, either coming from the free stream or from the wall) are here displayed for the first time. Calculating such functions from a numerical solution of the instability equations would require repeating the calculation for each of a complete set of different initial and boundary conditions; although numerical simulations of the Görtler instability abound in the literature, such a systematic screening has never been attempted. Here, instead, we calculate the Green's functions directly from a numerical solution of the adjoint of the linearized boundary-layer equations, which exploits the fact that the direct and adjoint parabolic problems have opposite directions of stable time-like evolution. The Green's functions can thus be obtained by marching backward in time at the same computational cost as a single forward-in-time integration of the direct problem. The backward-in-time technique is not limited to the Görtler problem; quantitative receptivity calculations for other types of instability can easily be envisioned.

1. Introduction

The original analysis (Görtler 1941) of the curvature-excited streamwise vortices that have become known as Görtler vortices was based on a heuristic extension of the theory of parallel centrifugal instabilities of the Taylor and Dean type (see e.g. Saric 1994 for a recent review). However, the flow cannot be treated as parallel in the initial region of G of order unity where the Görtler instability originates from external disturbances. This is why a study of the generation of Görtler vortices cannot be performed by local mode analysis but rather requires a numerical solution of the linearized boundary-layer equations, according to the method started by Hall (1983). For instance, the evolution of free-stream disturbances (such as those that may be caused by upstream screens) into Görtler vortices was studied by Hall (1990) and by Bottaro, Klingmann & Zebib (1996), whereas the evolution of wall-induced disturbances into Görtler vortices is considered in Denier, Hall & Seddougui (1991), Bassom & Hall (1994), Bertolotti (1993), Bassom & Seddougui (1995), and Bottaro &

† Present address: Institut de Mécanique des Fluides de Toulouse, UMR 5502, Université Paul Sabatier, 118 route de Narbonne, 31062 Toulouse Cedex 4, France.

Zebib (1997). In particular, Denier *et al.* (1991) considered a wall with different streamwise and spanwise roughness scales. The small and the $O(1)$ wavelength limits were examined with linear theory. Their $O(1)$ results were later extended and corrected by Bassom & Hall (1994), who indicated that distributed roughness is a very efficient means of vortex generation. Bertolotti (1993) solved, by a linear parabolized streamwise marching technique, the equations for the flow over concave surfaces with streamwise-aligned wall corrugations. This riblet-like wall was found to be very conducive to the formation and development of vortices, even when the riblet wavelength was different from that of the inlet vortex. Bertolotti also found that vortices are receptive to the wall forcing over an extended streamwise distance. Bassom & Seddougui (1995) studied the relative effectiveness of a given wall perturbation in exciting a Görtler rather than a crossflow instability in the presence of a small spanwise velocity component. Bottaro & Zebib (1997) performed a comparative study of some different wall-roughness configurations used as Görtler vortex generators.

The numerical approach generally adopted in Görtler receptivity studies has the advantage that the nonlinear saturation stage of the instability can be quite easily included, but the drawback that the computation must be repeated for every new initial disturbance, thus making it prohibitively time-consuming to answer such basic receptivity questions as which kind of disturbance is most effective in generating Görtler vortices and what thresholds must be imposed on ambient noise if one wants to avoid them. Indeed, an answer to such questions is not available in any of the aforementioned papers. On the other hand, within the limits of a linearized approach, receptivity questions do in principle possess a general quantitative answer. For, in a linear setting, the final mode amplitude in the large-G range (where local modes distinguished from each other do exist) must be a linear functional of the initial conditions, expressible as the integral of the product of the initial conditions times a suitable Green's function. The receptivity can, therefore, be quantitatively characterized by assigning this Green's function.

In this paper we take the calculation of the Green's function as our goal, and do it by first deriving a differential equation obeyed by the Green's function itself and then solving this equation by numerical means. The difference with the previous approach is that the numerical calculation has to be performed just once; after that, the influence of any initial condition on the final mode amplitude can be directly expressed through the Green's function, and the analysis of the effects of given, deterministic or random, perturbation sources becomes very easy.

2. Mathematical description of the Görtler problem

The centrifugal instability of the boundary layer over a concave wall discovered by Görtler in 1941 consists of steady longitudinal vortices which alternate in the spanwise direction. It occurs in a high-Reynolds-number boundary layer in the presence of a relatively small longitudinal curvature, so that the underlying span-independent mean velocity profile is (at leading order in the inner–outer expansion) unaffected. The simplest instance of Görtler instability takes place over a sharp-edged plate of constant radius of curvature in the absence of external pressure gradient, and we shall restrict ourselves in the following to this case for the sake of definiteness, although the generalization to variable radius of curvature and pressure gradient presents neither conceptual nor computational difficulty.

We shall describe the Görtler phenomenon by means of the linearized steady three-dimensional boundary-layer equations in the form

$$u_x + v_y + w_z = 0, \tag{1a}$$

$$Uu_x + U_x u + Vu_y + U_y v = u_{yy} + u_{zz}, \tag{1b}$$

$$Uv_x + V_x u + Vv_y + V_y v + 2G^2 Uu + p_y = v_{yy} + v_{zz}, \tag{1c}$$

$$Uw_x + Vw_y + p_z = w_{yy} + w_{zz}. \tag{1d}$$

Here x is the longitudinal boundary-layer coordinate made dimensionless with respect to an arbitrary reference length L, y and z are the wall-normal and spanwise coordinates made dimensionless with respect to the representative boundary-layer thickness $\delta = Re^{-1/2} L$, where $Re = LU_\infty/\nu$ is the (assumed large) longitudinal Reynolds number; accordingly, the longitudinal velocities U and u are made dimensionless with respect to the free-stream velocity U_∞ and the wall-normal and spanwise velocities with respect to $Re^{-1/2} U_\infty$. The unperturbed velocity components $U(x, y)$ and $V(x, y)$ are obtained from the Blasius solution for the unperturbed flat-plate boundary layer, while u, v, w and p represent velocity and pressure perturbations in the same boundary-layer scaling. The Görtler number G represents a non-dimensionalized curvature of the wall, of radius R, according to the definition $G^2 = Re^{1/2} L/R$, i.e. $G = L^{3/4}(U_\infty/\nu)^{1/4} R^{-1/2}$. The derivation of equations (1) can be found e.g. in Bottaro & Luchini (1996) and will not be repeated here. Historically, this formulation of the Görtler problem goes back to Floryan & Saric (1979, 1982) and Hall (1983). Indeed, these are nothing more than the general equations of a three-dimensional boundary layer (Carrier 1946; Moore 1956) with the addition of a curvature term $2G^2 Uu$.

Since the unperturbed flow represented by $U(x, y)$ and $V(x, y)$ is independent of z, it is expedient to Fourier-transform equations (1) with respect to z, thus obtaining

$$u_x + v_y - \mathrm{i}\beta w = 0, \tag{2a}$$

$$Uu_x + U_x u + Vu_y + U_y v = u_{yy} - \beta^2 u, \tag{2b}$$

$$Uv_x + V_x u + Vv_y + V_y v + 2G^2 Uu + p_y = v_{yy} - \beta^2 v, \tag{2c}$$

$$Uw_x + Vw_y - \mathrm{i}\beta p = w_{yy} - \beta^2 w, \tag{2d}$$

where the spanwise wavenumber β is non-dimensionalized with respect to $1/\delta = (U_\infty/L\nu)^{1/2}$. Equations (1) and (2) are parabolic and, just like the two-dimensional boundary-layer equations, require boundary conditions that specify u, v and w at the wall $y = 0$ and u, w and p (but not v) for $y \to \infty$. They also require initial conditions in x, the character of which is quite different from that of the conditions that must be assigned to the original Navier–Stokes equations. Indeed, the boundary-layer approximation changes the character of the Navier–Stokes equations from elliptic to parabolic, and simultaneously changes the number of initial conditions needed to form a well-posed problem. In two dimensions, and under the assumption that u never becomes negative, the boundary-layer equations only require one initial condition (for u, say, or equivalently for the streamfunction ψ) at a given position $x = x_0$ in order to make the solution determined for $x > x_0$. In three dimensions, two initial conditions must be given, by assigning, for instance, u and v (Hall 1983) or any other two equivalent quantities.

3. Forward numerical solution of the boundary-layer equations

It is possible to constrain equations (2) to having real coefficients by introducing $\bar{w} = \mathrm{i}\beta w$; in addition, the system can be put in a conservative form by suitably

combining the continuity equation with the other (this will become instrumental when we later deal with the leading edge). The system then becomes

$$u_x + v_y - \bar{w} = 0, \tag{3a}$$

$$(Uu)_x + Vu_y + U_y v = u_{yy} - \beta^2 u, \tag{3b}$$

$$(Vu + Uv)_x + (2Vv)_y - V\bar{w} + 2G^2 Uu + p_y = v_{yy} - \beta^2 v, \tag{3c}$$

$$(U\bar{w})_x + (V\bar{w})_y + \beta^2 p = \bar{w}_{yy} - \beta^2 \bar{w}, \tag{3d}$$

and the numerical solution may be set up in real variables. Equations (3) have been discretized by second-order central differences in y and either first- or second-order backward differences in x, on a regular unevenly spaced mesh in which $\bar{w}$ and p are staggered by half a y-step with respect to u and v. The system of finite-difference equations resulting from the discretization can be expressed as

$$(\boldsymbol{A}_n + \Delta x \boldsymbol{B}_n) \cdot \boldsymbol{q}_n = \boldsymbol{A}_{n-1} \cdot \boldsymbol{q}_{n-1}, \tag{4a}$$

or

$$(1.5\boldsymbol{A}_n + \Delta x \boldsymbol{B}_n) \cdot \boldsymbol{q}_n = 2\boldsymbol{A}_{n-1} \cdot \boldsymbol{q}_{n-1} - 0.5\boldsymbol{A}_{n-2} \cdot \boldsymbol{q}_{n-2} \tag{4b}$$

(respectively for first- and second-order differences in x). Here $x = n\,\Delta x$, the numerical vector $\boldsymbol{q}$ includes, at alternating positions, the four unknowns u, v, $\bar{w}$, p calculated at successive discretization points in y, and

$$\boldsymbol{A} \cdot \boldsymbol{q} = (u, Uu, Vu + Uv, U\bar{w}), \tag{5}$$

$$\boldsymbol{B} \cdot \boldsymbol{q} = (\text{finite difference form of } \{(v_y - \bar{w}), (Vu_y + U_y v - u_{yy} + \beta^2 u), [(2Vv)_y - V\bar{w} + 2G^2 Uu + p_y - v_{yy} + \beta^2 v], [(V\bar{w})_y + \beta^2 p - \bar{w}_{yy} + \beta^2 \bar{w}]\}. \tag{6}$$

To monitor the development of the instability one typically defines a perturbation energy, for example

$$E(x) = \int u^2(x, y)\,\mathrm{d}y \tag{7}$$

and introduces a dimensionless growth rate $\tilde{\sigma}$ as

$$\tilde{\sigma} = \frac{x}{2E}\frac{\mathrm{d}E}{\mathrm{d}x}. \tag{8}$$

The position of 'neutral' stability is defined by the value of x for which $\tilde{\sigma}$ vanishes: since a Görtler number $G_x = Gx^{3/4}$ and a wavenumber $\beta_x = \beta x^{1/2}$ are associated with each x, a 'neutral stability curve' in the (β_x, G_x)-plane can be constructed. Hall (1983) observed that the initial perturbation distributions u_0 and v_0 play a crucial role in the definition of the neutral curve; as a consequence he showed that the concept of a unique neutral curve is not tenable. In addition, Goulpié, Klingmann & Bottaro (1996) have demonstrated that even the definition of energy has profound repercussions on the location of the neutral points.

If, however, one calculates the evolution of the disturbance farther into the region of the (β_x, G_x)-plane where amplification is taking place, rather than solely looking for the neutral curve, one finds that with increasing G_x the amplification curves corresponding to different initial conditions do tend to coalesce with each other. This is borne out in figure 1, which shows the disturbance energy as a function of x (and G_x) and the final disturbance profiles for four initial disturbances chosen so as to represent four very different initial conditions. It can be observed that for G_x greater than about 7 the energy curves become almost indistinguishable from each other. The disturbance profiles also look very similar in this region. It thus appears that some kind of universal

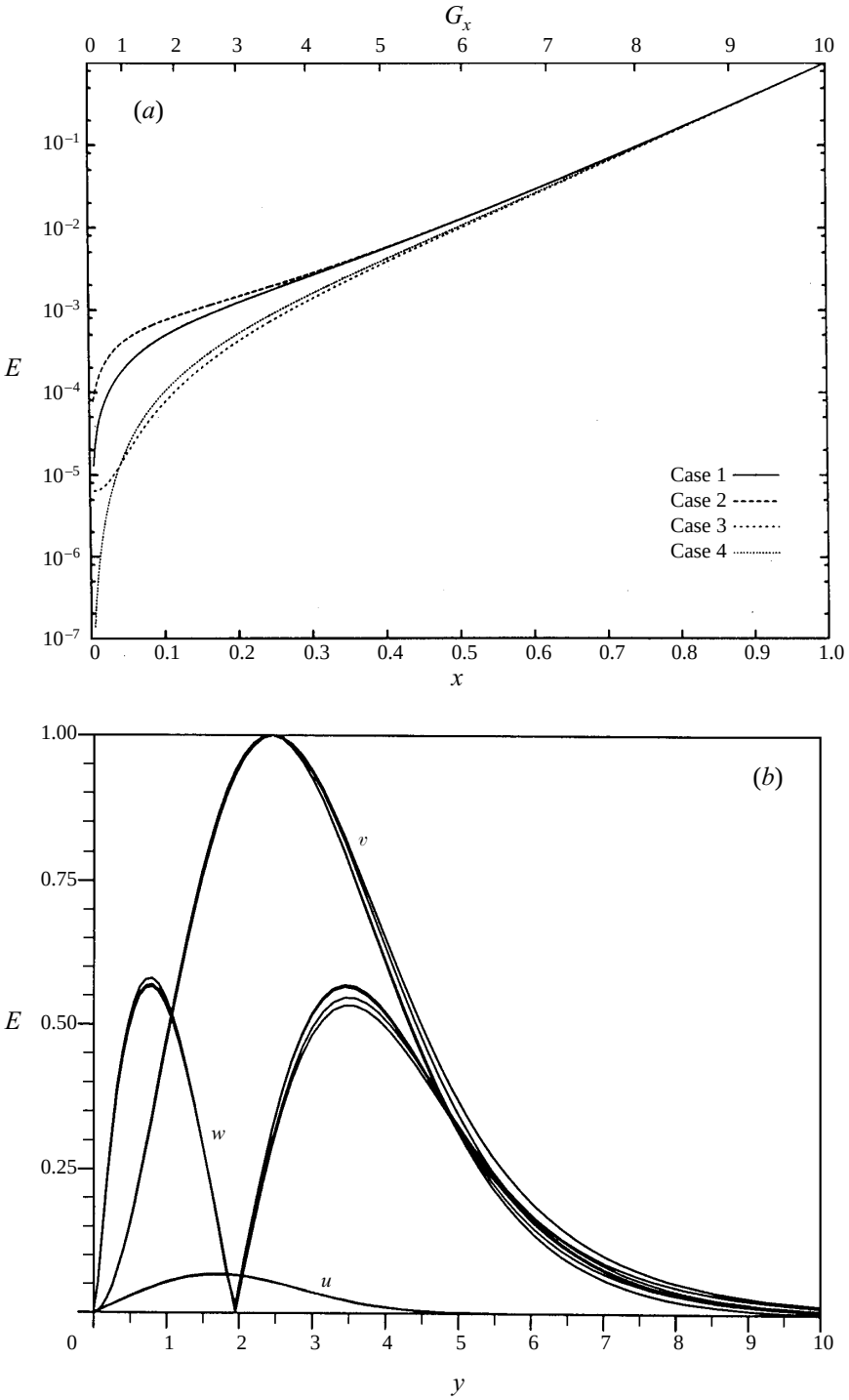

FIGURE 1. (*a*) Energy growth and (*b*) final u, v and w profiles for $\beta = 0.8$, $0 < G_x \leqslant 10$, and four different initial conditions: Case 1, $u_0 = 1$ on the first grid point above the wall, $v_0 = 0$; Case 2, $u_0 = 0$, $v_0 = 1$ on the first grid point above the wall; Case 3, $u_0 = yU_y$, $v_0 = 0$; Case 4, $u_0 = 0$, $v_0 = yU_y$.

behaviour (a *mode*) is approached in this range of Görtler numbers. Note that the existence of local modes was proved a long time ago by Hall (1982) in the part of the (β_x, G_x)-plane where the right-hand branch of the neutral curve is encountered, that is when amplification ends and turns back into damping again. It appears, however, that local modes can be defined even earlier than that. This is the object of a separate paper (Bottaro & Luchini 1998).

For the present purposes, it is enough to retain as an empirical observation that for $G_x > 7$ a universal disturbance shape is approached, up to an undetermined coefficient which determines the energy, in the numerical solution of equations (3). This coefficient must, of course, be a linear function of the initial conditions, since the problem is linear, and therefore calculating the coefficient will give a precise definition of the receptivity of Görtler vortices to initial conditions. Incidentally, it should be pointed out that $G_x = 7$ is well within the range of Görtler numbers of most experimental and numerical analyses available in the literature. Recent nonlinear calculations (Bottaro *et al.* 1996) and experiments (Pexieder 1996) – both performed in a fairly standard disturbance environment – show that the quasi-exponential growth characteristic of the linear amplification phase persists up to G_x of about 15.

4. Fundamental properties of the Green's function of a parabolic problem

Given a parabolic equation, formally represented in terms of the positive-definite operator $\mathbf{L}$ as

$$f_x = \mathrm{L}\cdot f, \tag{9}$$

it is always possible to introduce the adjoint equation

$$h_x = -\mathrm{L}^+\cdot h, \tag{10}$$

with the property that

$$(h\cdot f)_x = 0 \tag{11}$$

immediately proved by adding equation (9) scalarly multiplied by h to equation (10) scalarly multiplied by f, and using the defining property of adjoint operators that $h\cdot \mathrm{L}\cdot f = f\cdot \mathrm{L}^+\cdot h$. Integrated over a finite distance, equation (11) shows that h has the role of a Green's function for equation (9). For, if we choose h so that it assumes the form of a δ-function at a certain downstream abscissa x_f, we can write

$$\begin{aligned} f(x_f, y_f) &= \int_0^\infty \delta(y-y_f) f(x_f, y)\,\mathrm{d}y = \int_0^\infty h(x_f, y) f(x_f, y)\,\mathrm{d}y \\ &= \int_0^\infty h(x_i, y) f(x_i, y)\,\mathrm{d}y, \end{aligned} \tag{12}$$

and therefore we can calculate the value of f at the point (x_f, y_f) from the scalar product of the initial condition $f(x_i, y)$ times the Green's function $h(x_i, y)$. Moreover, the character of equation (10) is that of a parabolic equation with a negative-definite right-hand side, so that its intrinsic direction of stable evolution is reversed, and the problem of propagating the Green's function upstream from a δ-function condition given at x_f is well-posed.

More generally, given any linear functional of the final f that can be expressed as an integral (possibly in the sense of distributions as in the previous example), namely

$$\Phi = \int_0^\infty \phi(y) f(x_f, y)\,\mathrm{d}y, \tag{13}$$

we can recast Φ as a functional of the initial condition $f(x_i, y)$ by using as a Green's function the solution h_ϕ of equation (10) that equals $\phi(y)$ at x_f:

$$\Phi = \int_0^\infty h_\phi(x_i, y) f(x_i, y)\, \mathrm{d}y. \tag{14}$$

In all such cases, instead of propagating the solution of equation (9) forward in the time-like direction of the variable x and repeating the calculation for a number of different initial conditions, we need only propagate the solution of the adjoint equation (10) *backward in time* just once in order to get h_ϕ; formula (14) will then yield the value of Φ for every possible initial f. Below it will be seen that integrating equation (10) numerically is not any more difficult than integrating equation (9).

It may be noted that in the special case when the operator L is independent of the variable x, and therefore equation (9) admits simple eigensolutions proportional to $\mathrm{e}^{\sigma x}$ for suitable (generally complex) eigenvalues of σ, equation (12) reduces to the ordinary decomposition of the initial condition $f(x_i, y)$ in eigenfunctions of the operator L using the adjoint eigenfunctions as projection operators. This type of decomposition was recently used in a receptivity study of the Orr–Sommerfeld problem (Hill 1995). However, a local definition of the transverse eigenfunctions is not sufficient in the Görtler problem, because the most important disturbances act in a region where local eigenfunctions cannot be introduced. It then becomes essential to observe that equations (12) and (14) are valid for *any* operator L, whatever its x-dependence. A very compact alternative demonstration of this is offered by the use of the evolution operator U_{fi}, formally defined as that linear operator that relates the final profile $f_f(y) = f(x_f, y)$ to the initial condition $f_i(y) = f(x_i, y)$, *as* $f_f = \mathrm{U}_{fi} \cdot f_i$. Using a scalar-product notation for integrals such as equations (13) and (14), one can quickly derive that

$$\Phi = \phi \cdot f_f = \phi \cdot \mathrm{U}_{fi} \cdot f_i = h_\phi \cdot f_i, \tag{15}$$

where $h_\phi = \phi \cdot \mathrm{U}_{fi} = (\mathrm{U}_{fi})^+ \cdot \phi$. It should be evident that equation (15) does not require separability of either the operator L or U.

5. Backward formulation of the Görtler instability problem

It remains to be determined which particular downstream starting condition must be given to equation (10) in order to produce the appropriate Green's function that has the amplitude of the dominant mode as functional Φ. The answer is very easy, as a simplified example will illustrate. Let us consider the heat diffusion process in a finite slab with isothermal walls, i.e. the equation

$$f_t = f_{yy} \tag{16}$$

with boundary conditions $f(t, 0) = f(t, 1) = 0$. This equation admits separable modes of the form $f_n = \sin(n\pi y) \exp(-n^2\pi^2 t)$, $n \geqslant 1$; therefore with increasing t the solution produced by a 'generic' initial condition (provided only that it has a non-zero component in the first mode) tends to the asymptotic behaviour determined by the first mode alone, $\sin(\pi y) \exp(-\pi^2 t)$. The adjoint equation

$$h_t = -h_{yy} \tag{17}$$

with conditions $h(t, 0) = h(t, 1) = 0$ has separable modes given by $h_n = \sin(n\pi y) \exp(n^2\pi^2 t)$. The Green's function produced by a 'generic' starting condition tends with

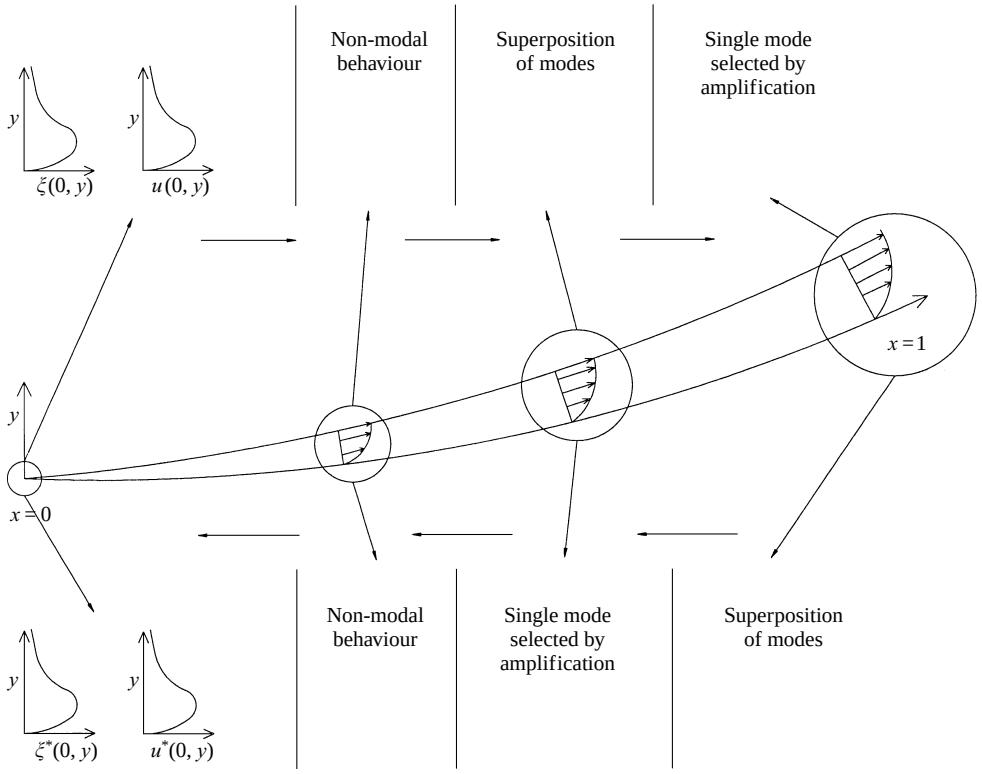

FIGURE 2. Schematic of the generation process for direct (top) and adjoint modes. The quantities u, ξ, u^*, ξ^* are introduced in §7.

decreasing t to the first mode $\sin(\pi y)\exp(\pi^2 t)$, i.e. to the adjoint eigenfunction needed to extract the first-mode component of the initial f.

This state of affairs is quite general. Whenever the operator $\mathbf{L}$ is separable, the same eigenvalue will govern the behaviour *with increasing* t of a given eigenfunction of equation (9) and the behaviour *with decreasing* t of the corresponding eigenfunction of equation (10). Therefore, an arbitrary initial condition, provided only that it is given sufficiently far downstream, will let the backward-marched solution of equation (10) converge to the adjoint eigenfunction of the leading mode. This is equally true in a situation, like that of Görtler vortices, in which separable modes exist only asymptotically in the limit of large x. In the same region where these modes exist, the backward-marched solution of the adjoint equation will tend to select the adjoint eigenfunction of the leading mode; continuing the solution all the way back will yield the Green's function that expresses the receptivity of the leading mode. This situation is schematically depicted in figure 2.

A slightly different but equivalent argument can also be given without assuming *a priori* that exact or approximate modes exist: if for any reason the solution of equation (9) tends to be attracted by one and the same functional form $f_0(y)$ with increasing x, independently of the initial condition except for an amplitude factor A, namely $f(x_f, y) = Af_0(y)$, then equation (11) allows this amplitude factor to be calculated from an arbitrary solution of equation (10) as

$$A = \int_0^\infty h(x_i, y) f(x_i, y)\,\mathrm{d}y \Big/ \int_0^\infty h(x_f, y) f_0(y)\,\mathrm{d}y. \tag{18}$$

Of course, equation (18) can only hold for an arbitrary Green's function h insofar as h conversely tends to one and the same functional form with decreasing x independently of the starting condition given at x_f. This limiting functional form is the receptivity.

6. Numerical computation of the Green's function

The standard procedure for extracting the adjoint system from equations (3) begins by multiplying each of the four equations by suitable, yet to be defined, weight functions, denoted here by $a(x,y)$, $b(x,y)$, $c(x,y)$ and $d(x,y)$, and then adding and integrating in y. By successive integrations by parts it is easily found that

$$\begin{aligned}\frac{\mathrm{d}}{\mathrm{d}x}\int_0^\infty [&au+bUu+c(Vu+Uv)+dU\bar{w}]\,\mathrm{d}y\\ &+|av+bVu-bu_y+b_y u+2cVv+cp-cv_y+c_y v+dV\bar{w}-d\bar{w}_y+d_y\bar{w}|_{y=0}^{y=\infty}\\ &+\int_0^\infty [-a_x u-a_y v-a\bar{w}-b_x Uu-(bV)_y u+bU_y v-b_{yy}u+b\beta^2 u\\ &-c_x(Vu+Uv)-2c_y Vv-cV\bar{w}+2G^2 cUu-c_y p-c_{yy}v+\beta^2 cv\\ &-d_x U\bar{w}-d_y V\bar{w}+d\beta^2 p-d_{yy}\bar{w}+d\beta^2\bar{w}]\,\mathrm{d}y=0. \end{aligned}\tag{19}$$

An integral relation verified by an arbitrary solution of the original problem (3) is then generated by choosing the undetermined coefficients a, b, c and d in such a way that each term of equation (19) is separately equal to zero. One thus obtains that the scalar product

$$s=\int_0^\infty [au+bUu+c(Vu+Uv)+dU\bar{w}]\,\mathrm{d}y \tag{20}$$

is constant with x provided a, b, c, d represent a solution of the system

$$a_x+Ub_x+Vc_x+(Vb)_y+b_{yy}-\beta^2 b=2G^2 Uc, \tag{21a}$$

$$Uc_x+2Vc_y+c_{yy}-\beta^2 c=U_y b-a_y, \tag{21b}$$

$$Ud_x+Vd_y+d_{yy}-\beta^2 d=-a-Vc, \tag{21c}$$

$$c_y=\beta^2 d, \tag{21d}$$

with boundary conditions $b=c=d=0$ at $y=0$ and $a+2Vc+c_y=0$ for $y\to\infty$ (which, together with the boundary conditions of the direct problem, $u=v=\bar{w}=0$ at $y=0$ and $u=\bar{w}=p=0$ for $y\to\infty$, nullify the second term of equation (19)). By use of equation (21d) and the boundary conditions, the scalar product defined by equation (20) can also be rewritten with two terms only as

$$s=\int_0^\infty (u^*u+\Xi^*\Xi)\,\mathrm{d}y, \tag{22}$$

where $u^*=a+bU$, $\Xi^*=-\mathrm{i}c/\beta$ and

$$\Xi=(Uw)_y+\mathrm{i}\beta(Vu+Uv). \tag{23}$$

At this point it would seem necessary, from the computational point of view, to discretize the 'backward' system of equations (21) by finite differences in a similar manner as for the 'forward' system (3). However, there is an even easier way. The idea of computing a Green's function as a particular solution of the adjoint system of

equations applies to a discrete as well as to a continuous system: since we already have available a discretization of the forward problem, formulating the discrete version of the adjoint problem becomes just a matter of matrix transposition.

In fact, multiplying equation (4*a*) by a yet to be defined coefficient vector $\boldsymbol{p}_{n-1}$ and subtracting from both sides $\boldsymbol{p}_n \cdot \boldsymbol{A}_n \cdot \boldsymbol{q}_n$ (the equivalent of integration by parts) yields

$$\boldsymbol{p}_{n-1} \cdot (\boldsymbol{A}_n + \Delta x \boldsymbol{B}_n) \cdot \boldsymbol{q}_n - \boldsymbol{p}_n \cdot \boldsymbol{A}_n \cdot \boldsymbol{q}_n = \boldsymbol{p}_{n-1} \cdot \boldsymbol{A}_{n-1} \cdot \boldsymbol{q}_{n-1} - \boldsymbol{p}_n \cdot \boldsymbol{A}_n \cdot \boldsymbol{q}_n. \tag{24}$$

It follows that

$$s = \boldsymbol{p}_n \cdot \boldsymbol{A}_n \cdot \boldsymbol{q}_n \tag{25}$$

is independent of n provided the vector $\boldsymbol{p}_n$ is obtained from the difference equation

$$(\boldsymbol{A}_n + \Delta x \boldsymbol{B}_n)^T \cdot \boldsymbol{p}_{n-1} = \boldsymbol{A}_n^T \cdot \boldsymbol{p}_n. \tag{26}$$

The analogy with equations (10) and (11) is remarkable: equation (26) is the discrete adjoint equation that must be iterated backward (that is, for n decreasing) in order to determine the Green's function. As anticipated, it can be derived from the forward discretized equations by a simple transposition of the matrices defined in equations (5) and (6); as an additional simplification, wall and free-stream boundary conditions need not be handled separately if the boundary conditions for the forward problem are initially included in the appropriate rows of matrix $\boldsymbol{B}$. An essentially similar procedure yields the discrete backward-marching difference equation corresponding to the second-order approximation (4*b*).

In order to recover the continuous Green's function from the discrete vector $\boldsymbol{p}_n$, we need only equate a discrete approximation of equation (22) to equation (25), identifying the coefficient $u^*\Delta y$ of u and the coefficient $\Xi^*\Delta y$ of Ξ in the product $\boldsymbol{p}_n \cdot \boldsymbol{A}_n \cdot \boldsymbol{q}_n$.

We note that, even if equation (4*a*) were an arbitrary discrete equation and not an approximation of a continuous problem, equation (26) would correctly define a Green's function for it: whenever $\boldsymbol{p}_n$ is calculated by iterating equation (26) backwards from a δ-function starting condition at $n = N$ (a vector $\boldsymbol{p}_N$ with all components but one zero), the scalar product $\boldsymbol{p}_N \cdot \boldsymbol{A}_N \cdot \boldsymbol{q}_N$ (a single component of $\boldsymbol{A}_N \cdot \boldsymbol{q}_N$) equals $\boldsymbol{p}_0 \cdot \boldsymbol{A}_0 \cdot \boldsymbol{q}_0$ for any $\boldsymbol{q}$ that obeys equation (4*a*). Therefore equations (14) and (18) remain valid even for discontinuous solutions, provided only that such solutions are properly captured by the discretization of the forward problem.

7. The receptivity of Görtler vortices to free-stream disturbances

7.1. *Formulation*

Externally generated small disturbances can arrive from the free stream into the boundary layer in two forms: as acoustic waves, which propagate in all directions and are accompanied by a time-varying irrotational velocity field; or as vorticity waves which move along streamlines like material particles. The former are inherently high-frequency disturbances (in order to have a spanwise wavenumber of β they must have a frequency of at least βa, with a being the speed of sound), and on an ideal plate of infinite span do not couple to steady or quasi-steady Görtler instabilities. The second can only arrive from directly upstream of the plate along the streamlines which eventually enter the boundary layer, and therefore appear in the mathematical formulation as initial conditions at the leading edge of the plate. Here, however, we meet a difficulty: at the leading edge of the plate, $x = 0$, the solution of the boundary-layer equations that corresponds to a uniform impinging stream (the Blasius similarity

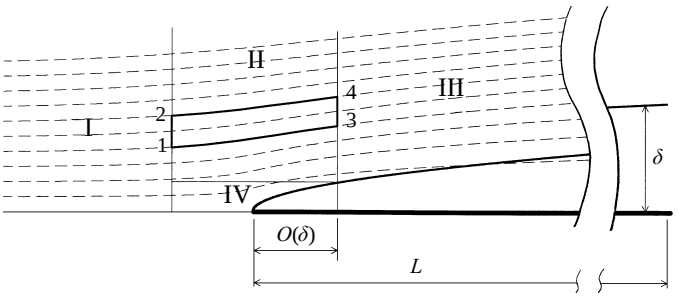

FIGURE 3. Structure of the boundary layer near the leading edge.

solution) has a singularity in which V behaves as $x^{-1/2}$, and the boundary-layer approximation itself becomes invalid. Therefore, in order to investigate the receptivity of Görtler vortices to free-stream disturbances, we must first be able to connect the properties of the boundary layer with those of the upstream oncoming disturbances, 'jumping over', so to speak, the discontinuity. The appropriate jump conditions to describe the initial region of a three-dimensional boundary layer were discussed and determined by Ting (1965), who did so in a general compressible-fluid setting. Since such conditions are essential to the interpretation of our results in terms of leading-edge receptivity, a brief re-derivation limited to the incompressible case will now be given.

Actually, several different scales of length must be distinguished in a neighbourhood of the leading edge. If L is the total length of the plate (or, equivalently, the downstream position at which we are measuring disturbance amplification), the final boundary-layer thickness $\delta = (L\nu/U)^{1/2}$ turns out to determine the y-range of disturbances to which the boundary layer is most sensitive, as will be seen from the numerical results, so that the structure of the leading-edge singularity must be investigated for disturbances characterized by a typical transverse scale δ_d comparable to δ. Near the leading edge, therefore, such disturbances are quite well separated in scale from the Blasius base flow, which has a typical scale of $(x\nu/U)^{1/2}$ with the local value of x, and are mostly carried along by the inviscid free stream above the boundary layer.

Equations (2), which require the scale in x to be much larger than the scale in y, can only be applied to disturbances for $x \quad \delta_d \approx \delta$, i.e. $x/L \quad (UL/\nu)^{-1/2}$. Nevertheless, in boundary-layer scaling $(UL/\nu)^{-1/2}$ is an infinitesimal quantity, so that the region near the leading edge where the approximation fails is perceived as a localized discontinuity. It should be noted that sufficiently upstream of the leading edge equations (2) recover their validity, with a base flow simply given by $U = 1$ and $V = 0$, and all that we actually need is a jump condition connecting the properties of the disturbance upstream of the discontinuity, for $x \quad -\delta$, with its properties downstream of the discontinuity, for $x \quad \delta$, much in the same way as when shock waves or shear layers are dealt with in inviscid fluid mechanics.

At a distance x of order δ from the leading edge there is a triple-deck structure, with a viscous inner deck for $0 < y \lesssim (\delta\nu/U)^{1/2} = L^{1/4}(\nu U)^{3/4}$ and an inviscid but rotational outer deck for $(\delta\nu/U)^{1/2} \quad y \lesssim \delta$. It is this outer deck that determines the coupling conditions we are interested in, the inner deck occupying only an infinitesimal portion of the disturbance cross-section. The situation is schematically depicted in figure 3.

The oncoming stream is uniform except for a superposed disturbance which is sufficiently small to be treated linearly, and is assumed to have a typical scale of length

$\delta_d \approx \delta \quad \nu/U_\infty$ in both the spanwise and wall-normal directions. The convection and slow diffusion of this disturbance in region I, at a negative $x \quad -\delta$, can be represented by the same boundary-layer equations (1), with a base flow represented by $U = 1$ and $V = 0$. Since these equations can be recast as

$$u_x = -(\gamma^2+\beta^2)\,u, \quad \xi_x = -(\gamma^2+\beta^2)\,\xi, \tag{27a, b}$$

with $\xi = w_y + \mathrm{i}\beta v$ representing the streamwise component of vorticity, we can distinguish two independent types of disturbance: u-disturbances (streaks) and ξ-disturbances (rolls). Each of these kinds of disturbance is accompanied by a crossflow with both v- and w-components; in the crossflow plane, they appear respectively as source–sink (irrotational) and vortical (divergence-free) velocity fields.

In regions II and IV, for $-\delta \leqslant x \leqslant \delta$ the longitudinal pressure gradient is no longer negligible, but in region II, for $y \quad (\delta\nu/U)^{1/2}$, viscosity is. In this region the governing equations are the inviscid Euler equations, and vorticity propagates along streamlines like an infinitesimal material segment. The streamlines themselves can be determined from, for instance, Kaplun's (1954) optimal coordinate solution.

Region II can be treated as a discontinuity on the boundary-layer scale. Rather than solving the linearized Euler equations pointwise in this region in order to follow the evolution of the perturbation along the inviscid streamlines, we can set up an integral momentum balance over a region like that denoted by 1–2–3–4 in figure 3, with two sides parallel to the y-axis and two sides formed by streamlines. Since there are no convective fluxes through the streamlines, we obtain

$$\int_{y_1}^{y_2} u\,\mathrm{d}y = \int_{y_3}^{y_4} u\,\mathrm{d}y, \tag{28a}$$

$$\int_{y_1}^{y_2} (2Uu+p)\,\mathrm{d}y = \int_{y_3}^{y_4} (2Uu+p)\,\mathrm{d}y, \tag{28b}$$

$$\int_{y_1}^{y_2} (Vu+Uv)\,\mathrm{d}y + \int_{1\text{–}2\text{–}3\text{–}4} p_y\,\mathrm{d}x\,\mathrm{d}y = \int_{y_3}^{y_4} (Vu+Uv)\,\mathrm{d}y, \tag{28c}$$

$$\int_{y_1}^{y_2} (Uw)\,\mathrm{d}y - \int_{1\text{–}2\text{–}3\text{–}4} \mathrm{i}\beta p\,\mathrm{d}x\,\mathrm{d}y = \int_{y_1}^{y_2} (Uw)\,\mathrm{d}y. \tag{28d}$$

Now we have that pressure is the same on the lines 1–2 and 3–4, because both far behind and far beyond the leading edge the pressure is constant and equal to the external pressure, and therefore disappears from equation (28b). Moreover, we can eliminate pressure between equations (28c) and (28d) by summing the first multiplied by $\mathrm{i}\beta$ to the second differentiated with respect to y. Since, in addition, the vertical displacement of the streamlines between these two planes is of order $(\delta\nu/U)^{1/2}$ and thus negligible with respect to δ, and relations (28) must hold for all possible choices of the two limiting streamlines, we obtain a classical jump condition between the lines 1–2 and 3–4 in the form

$$[u]_{1\text{–}2} = [u]_{3\text{–}4}, \tag{29a}$$

$$[Uu]_{1\text{–}2} = [Uu]_{3\text{–}4}, \tag{29b}$$

$$[(Uw)_y + \mathrm{i}\beta(Vu+Uv)]_{1\text{–}2} = [(Uw)_y + \mathrm{i}\beta(Vu+Uv)]_{3\text{–}4}, \tag{29c}$$

where, in the scaling appropriate to regions I and III, the planes 1–2 and 3–4 must be interpreted as being at an infinitesimal distance from each other. In other words,

equations (29) relate the limits for x going to zero from the left and from the right of certain flow properties. We thus see that u, Uu and the quantity in square brackets in equation (29c) (the same that we have already denoted by Ξ in equation (23)) must remain continuous across the leading edge $x = 0$. Other boundary-layer quantities, e.g. the velocity perturbation components v and w and the unperturbed V, are instead discontinuous here.

The two initial conditions that must be assigned to identify a solution of the boundary-layer equations (2) can thus be uniquely assigned even when the calculation is started from the leading edge, $x = 0$, provided care is taken in assigning the quantities that are continuous there. In fact, of the three jump conditions just determined the first two are equivalent, since the unperturbed velocity U is itself continuous, and therefore the perturbations of u and Ξ must be assigned at $x = 0$ to equal their free-stream values. The receptivities u^* and Ξ^* defined in the previous section assume at $x = 0$ the role of receptives to free-stream disturbances. In particular, since in the oncoming stream, where $U = 1$ and $V = 0$, Ξ reduces to the longitudinal vorticity ξ of equation (27b), the value of Ξ^* at $x = 0$ represents the receptivity to longitudinal vorticity disturbances, which we may call *roll receptivity* and denote by ξ^*, whereas the value of u^* at $x = 0$ represents the receptivity to longitudinal velocity disturbances, which we may call *streak receptivity*.

In order to obtain from equation (18) a quantitative definition of the receptivity to the two kinds of external disturbance just mentioned, we must still define a suitable normalization for the final disturbance f_0 which appears at the end of the plate. (The disturbance velocity profile is easily generated from a marching numerical solution of the direct equations, but only up to an undetermined multiplicative constant.) We have chosen to normalize the direct and the adjoint solutions in such a way that both the kinetic energy defined by equation (8a) and the scalar product s defined by equation (22) are of unit value at the exit $x = L$. Thus the scalar product s of equation (22) will automatically represent, for any given initial disturbance, the square root of the energy that the disturbance attains at the end of the plate.

7.2. *Numerical results*

Figure 4 provides an example of receptivity curves $u^*(y)$ and $\xi^*(y)$, obtained for a selection of values of G and β by marching the solution of the backward difference equation from $x = 1$ down to $x = 0$ and normalizing the result. It has been checked that the same curves turn up, within graphical accuracy, with several different initial conditions and different refinements of the discretization. It should be remembered, in order that this and subsequent figures may be interpreted correctly, that the position where the final disturbance is observed (and normalized at unit energy) has been taken as reference length L, and therefore the Görtler number has been calculated according to this length and the y-coordinate in the figure must be read in units of $(L\nu/U_\infty)^{1/2}$. It is not required that the plate should actually end at $x = L$ because of the parabolic character of the boundary layer.

Figure 4 gives some not previously available information, for instance that a spatially localized disturbance is most effective if it flies over the leading edge at a distance $y \approx 1$ and that, since there is no change in sign of either receptivity, disturbances travelling at different heights sum up in phase. Even more interestingly, figure 4 shows what an *optimal disturbance* should look like. Optimal disturbances, loosely defined as those disturbances that produce the maximum effect with the minimum effort, are being investigated for different kinds of fluid dynamic instabilities, in particular under those circumstances in which the non-orthogonality of modes plays

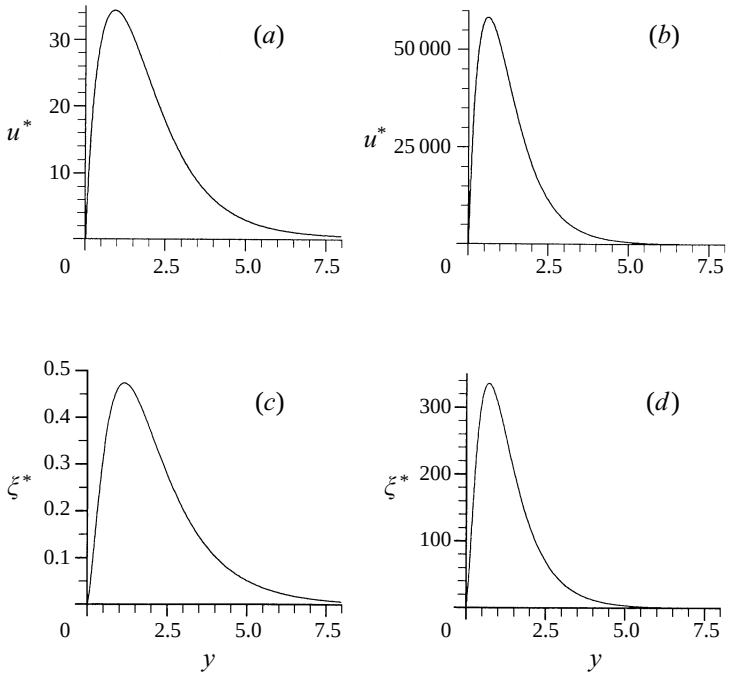

FIGURE 4. (*a*, *b*) Streak receptivity curves for (*a*) $(G, \beta) = (10, 0.80)$ and (*b*) (20, 1.22). (*c*, *d*) Roll receptivity curves for (*c*) $(G, \beta) = (10, 0.71)$ and (*d*) (20, 1.18). The values chosen for (G, β) correspond to optima, as in table 1.

a major role (Butler & Farrel 1992). Once the receptivity curve is available, the *effect* of a given disturbance is unequivocally measured by the integral of equation (22). For any suitable definition of the *effort*, it becomes a trivial matter to maximize the one given the other. For instance, if the effort required to create a streak disturbance is measured by its kinetic energy according to the definition (7), it is immediately seen that an optimal streak disturbance is one proportional to u^* itself. Similarly, if the effort required to create a roll disturbance is measured by the integral of ξ^2, an optimal roll disturbance is one proportional to ξ^*. The consequences of other definitions can easily be tested.†

Plots such as figure 4 can be repeated for different Görtler numbers G and spanwise wavenumbers β. A more comprehensive outlook of the receptivity properties in the z- and y-directions, however, comes from looking at the data in a two-dimensional wavenumber space. In fact, since there is no real distinction between the z- and y-directions upstream of the plate, the oncoming disturbance is more naturally thought of as a superposition of two-dimensional Fourier components in the plane β, γ of the z- and y-wavenumbers than as a mixed representation in β and y. From Parseval's theorem applied to equation (22), we see immediately that the receptivities $u^*(\beta, \gamma)$ and $\xi^*(\beta, \gamma)$ to such two-dimensional plane waves are quite simply the Fourier transforms

† As far as a relative comparison between streak receptivity and roll receptivity is concerned, it should be remembered that in boundary-layer variables the longitudinal and crossflow velocity components are normalized differently. Therefore, v, w and ξ should be multiplied by $Re^{-1/2}$ before they are energetically compared to u, and conversely u^* should be multiplied by $Re^{-1/2}$ in order to be compared to ξ^*. In the limit of $Re \to \infty$ the receptivity to streak disturbances eventually becomes negligible and only roll disturbances have to be taken into consideration. For finite Reynolds number, however, no general conclusion can be reached.

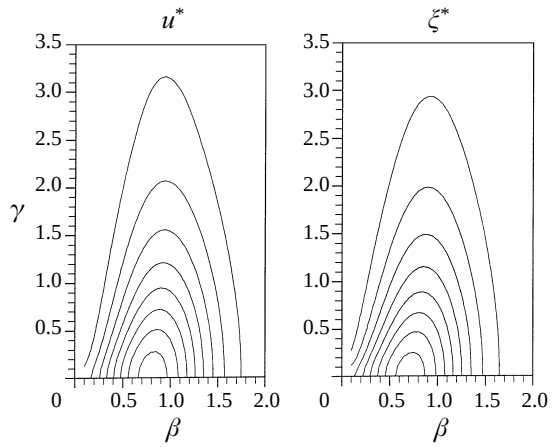

FIGURE 5. Contour plot in the spanwise–vertical wavenumber space of the free-stream receptivity. $G = 10$.

G	$\beta_{max\,u^*}$	$\beta_{max\,\xi^*}$
10	0.80	0.71
15	1.04	0.99
20	1.22	1.18
25	1.39	1.32
30	1.50	1.37

TABLE 1. Wavenumbers of maximum free-stream receptivity

of $u^*(\beta, y)$ and $\xi^*(\beta, y)$. Therefore in figure 5 we have plotted the level curves of the moduli of these Fourier transforms at $G = 10$, with the aim of picking up the wavenumber range of maximum receptivity. This maximum appears quite clearly located around $\beta = 0.8$, $\gamma = 0$ for the streak receptivity and at $\beta = 0.7$, $\gamma = 0$ for the roll receptivity. The fact that the isolines are somewhat oblong along γ indicates a relatively lower selectivity of Görtler vortices to wall-normal than to spanwise wavenumbers. If isotropically distributed random fluctuations are carried by the free stream, their effectiveness will mostly be governed by the spanwise wavenumber distribution. This result is consistent with the one obtained by Hall (1990), who performed forward simulations of equations (2) subject to leading-edge disturbance conditions of the type $u = \varepsilon \cos(\gamma y)\exp(\mathrm{i}\beta z)$, to model a grid upstream of the test section. Hall computed neutral curves and found that the most unstable disturbance is characterized by $\gamma = 0$. In the present work, the focus is not on marginal conditions (where G is typically small) but on the downstream solutions with large G. Once the spectral distribution of the Green's function is known, a scalar product with the spectral receptivity will quantitatively determine the amplitude of the generated vortex. Similar transfer function plots can easily be obtained for other values of G; the wavenumbers of maximum receptivity are collected in table 1. Notice that if the non-dimensional wavelength Λ is introduced, defined as

$$\Lambda = G\left(\frac{2\pi}{\beta}\right)^{3/2},$$

the wavelengths of maximum free-stream receptivity are all within the often quoted

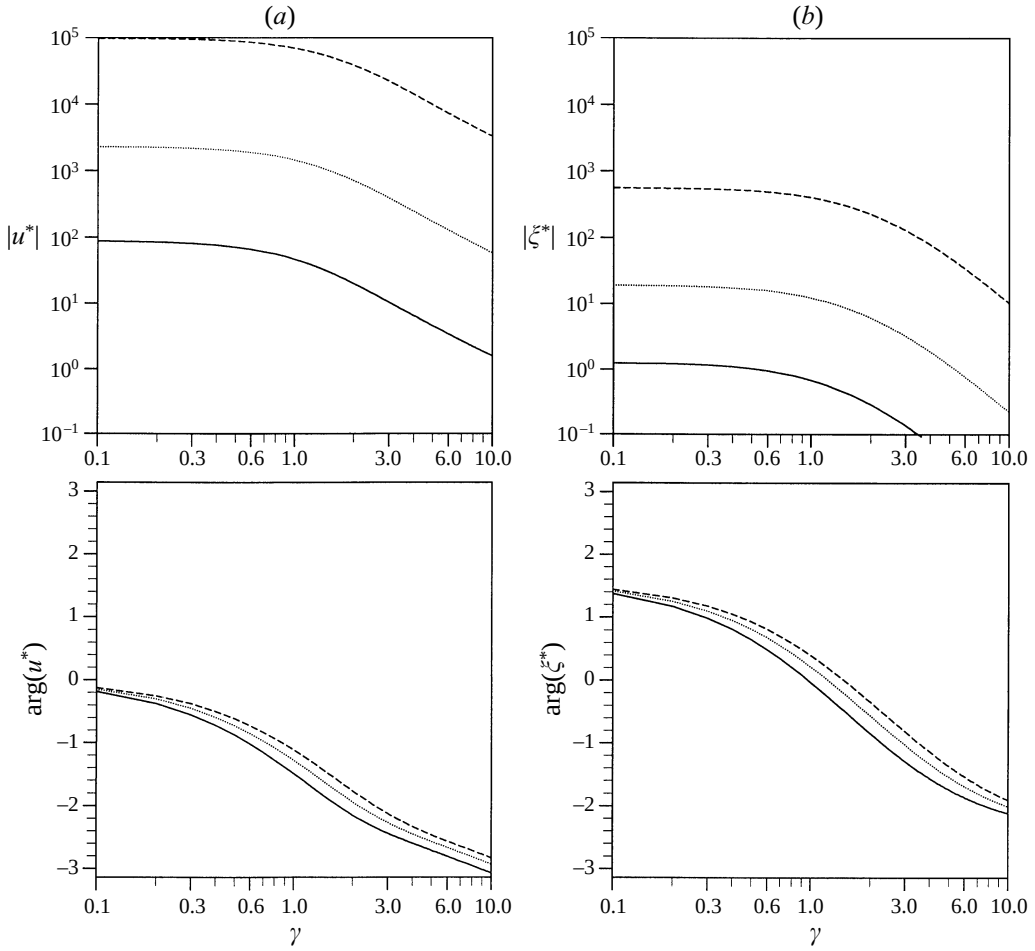

FIGURE 6. Modulus and phase of the wavenumber receptivity for streaks (*a*) and rolls (*b*), at each β_{max} from table 1 corresponding to $G = 10$ (solid lines), $G = 15$ (dotted lines) and $G = 20$ (dashed lines), as a function of the vertical wavenumber γ.

range $\Lambda \in [220, 270]$ (Bottaro *et al.* 1996). Constant-β and constant-γ cross-sections through the points of maximum are given in figures 6 and 7.

8. The receptivity of Görtler vortices to wall disturbances

8.1. *Formulation*

If the forward problem (2) is given homogeneous initial conditions and non-zero wall boundary conditions, the effect of disturbances coming from the wall can be studied. Since three boundary conditions are needed, one for each component of the velocity, three types of wall disturbance can be considered: *u*-, *v*- and *w*-disturbances. (The reader is referred e.g. to Bottaro & Zebib 1997 for a discussion of the relationship between velocity disturbances and wall imperfections.) As far as the adjoint problem is concerned, once the boundary conditions $u = v = w = 0$ are replaced by $u = u_w(x)$, $v = v_w(x)$ and $w = w_w(x)$ a non-zero contribution appears in the second line of

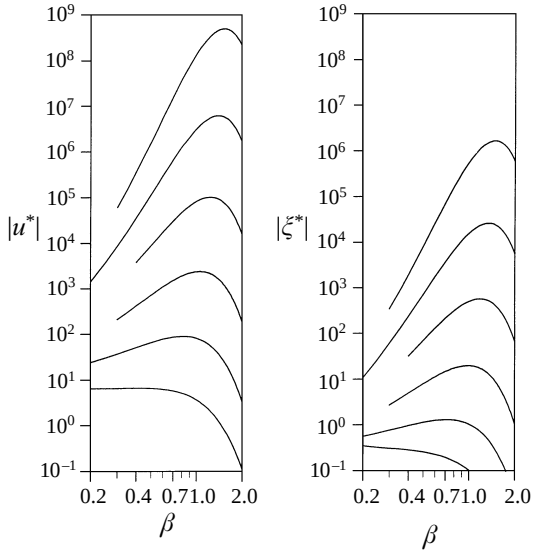

FIGURE 7. Modulus of the (real) wavenumber receptivity at $\gamma = 0$ as a function of β. G increases from 5 to 30 in steps of five, from the bottom to the top.

equation (19); with the coefficients a, b, c and d obeying the same differential equations and boundary conditions (21) as before, equation (19) now becomes

$$\frac{\mathrm{d}}{\mathrm{d}x}\int_0^\infty [au + bUu + c(Vu + Uv) + dU\bar{w}]\,\mathrm{d}y = [b_y u + (a + c_y)v + d_y \bar{w}]_{y=0}, \tag{30}$$

i.e. in terms of the scalar product s of equation (20),

$$s_f = s_i + \int_0^1 [b_y u_w + (a + c_y)v_w + d_y \bar{w}_w]\,\mathrm{d}x. \tag{31}$$

This formula replaces the statement that (in the absence of wall perturbations) the scalar product s remains constant. The effect of wall boundary conditions is represented through a boundary integral in the same way as the effect of initial conditions is represented by the initial integral s_i. The functions $b_y(x,0)$, $[a(x,0) + c_y(x,0)]$ and $\mathrm{i}\beta d_y(x,0)$ define the wall receptivities $u_w^*(\beta,x)$, $v_w^*(\beta,x)$ and $w_w^*(\beta,x)$, and can be obtained simultaneously with the initial-value receptivities at no additional computational cost.

By a similar argument, it can be easily shown that the functions a, b, c and d represent the receptivity to mass and momentum productions possibly introduced as external forcing terms in equations (3*a–d*) respectively.

8.2. *Numerical results*

Figure 8 shows the wall receptivity curves $u_w^*(\beta,x)$, $v_w^*(\beta,x)$ and $w_w^*(\beta,x)$ for representative values of G and β. It can be observed that receptivity is maximum at the leading edge and, like the initial-value receptivity, never changes sign. The fact that wall forcing is most effective at the leading edge was already noted by Bassom & Hall (1994), who investigated the effect of both an isolated roughness element (modelled by a delta-function at the wall) and distributed roughness (taken to vary like $\sin x$). Our result is, however, of a more comprehensive nature since receptivity curves such as those given in figure 8 automatically determine the shape of an optimal wall disturbance. In particular, if the effort required to create a velocity disturbance at the

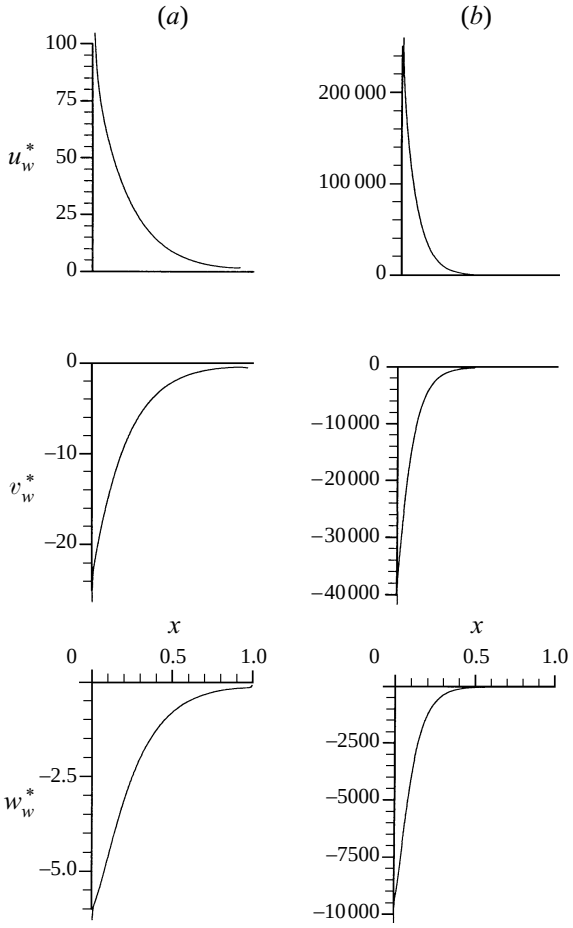

FIGURE 8. u, v and w wall receptivity curves for (a) $(G, \beta) = (10, 0.89)$ and (b) (20, 1.29). These values correspond to those of maximum u-receptivity at the given G, as in table 2.

wall is measured by its kinetic energy, an optimal u-disturbance is one proportional to u_w^*, a optimal v-disturbance is one proportional to v_w^* and an optimal w-disturbance is one proportional to w_w^*. We recall that u-disturbances are scaled differently from v- and w-disturbances and must be multiplied by a factor $Re^{1/2}$ before being compared to them.

If wall disturbances are represented by a superposition of sinusoidal components, the Fourier transform of each receptivity function becomes useful. Figure 9 shows the level curves of the moduli of these Fourier transforms in the plane α, β of the streamwise and spanwise wavenumbers at $G = 10$. Notice that, contrarily to what happened for the initial-value receptivities, wavelengths on the two axes are now not directly comparable because there is a ratio of $Re^{1/2}$ between their respective scales. Nevertheless, these curves still allow us to point out the wavenumber range of maximum receptivity, which occurs for $\alpha = 0$ (as also noted empirically by Bottaro & Zebib 1997 via forward nonlinear calculations) and β close to 1. For large β roughness is inefficient in stimulating Görtler vortices, as already remarked by Denier *et al.* (1991). The wavenumbers of maximum receptivity are collected in table 2 for some values of G. Constant-β and constant-α cross-sections through the points of maximum are given in figures 10 and 11.

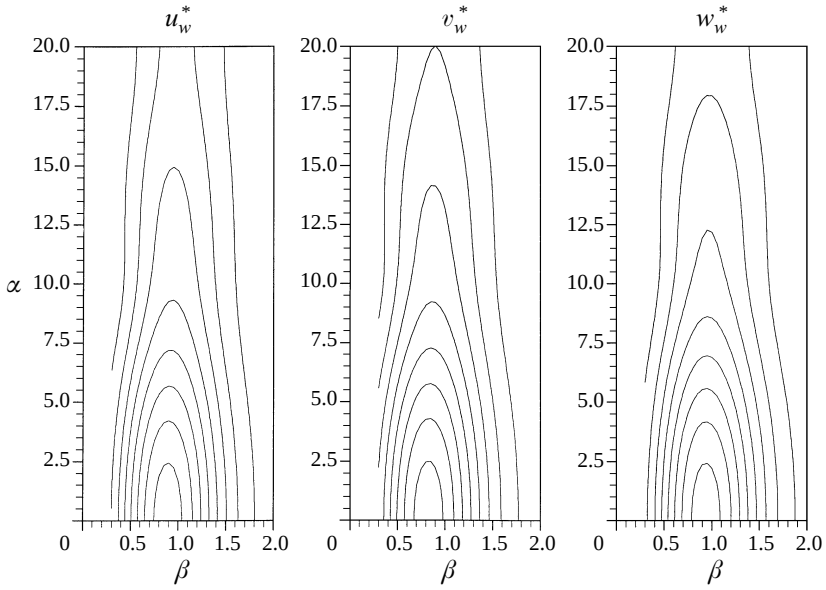

FIGURE 9. Contour plots of the receptivity in the spanwise–streamwise wavenumber space for u, v and w wall disturbances, from left to right. $G = 10$.

G	$\beta_{max u_w^*}$	$\beta_{max v_w^*}$	$\beta_{max w_w^*}$
10	0.89	0.81	0.94
15	1.10	1.05	1.15
20	1.29	1.22	1.20
25	1.42	1.39	1.32
30	1.55	1.51	1.49

TABLE 2. Wavenumbers of maximum wall receptivity

9. Conclusions

In this paper the first complete quantitative definition of the receptivity of the Görtler instability is given, by calculating the Green's functions that external (free-stream or wall-induced) disturbances must be scalarly multiplied by in order to yield the final amplitude of the most amplified instability mode.

Repeated numerical simulations for each of a complete set of different initial and wall conditions were avoided by calculating the Green's functions directly from the adjoint of the linearized boundary-layer equations. Since the direct and adjoint parabolic problems have opposite directions of stable time evolution, the Green's functions could thus be obtained by marching the numerical simulation backward in time. It might be said that, in this time-reversed approach to instability analysis, the disturbance is followed, in adjoint-function space, from the time when it is observed back to the time when it was generated. From the computational viewpoint this is a problem of the same order of difficulty as a single numerical integration of the forward system of equations, provided proper care is taken concerning the singularities that arise, under the boundary-layer approximation, at the leading edge of the plate.

The analysis of the receptivity curves shows a relatively smooth behaviour, with no change in sign of any of the five types of receptivity (to u and ξ free-stream disturbances

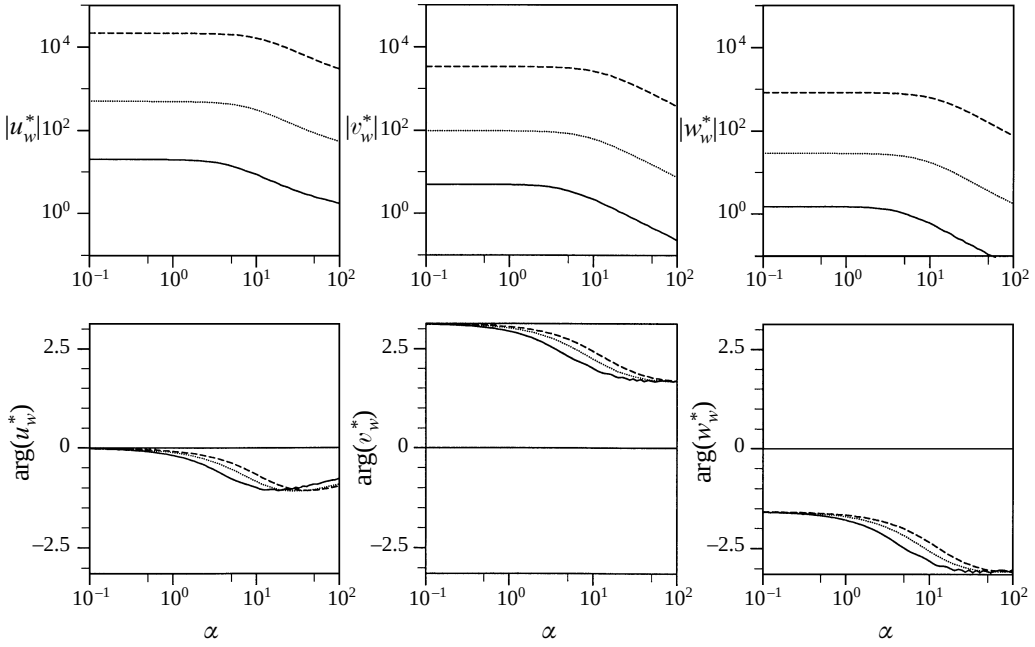

FIGURE 10. Modulus and phase of the wall wavenumber receptivity as a function of α. $G = 10$ (solid lines), $G = 15$ (dotted lines) and $G = 20$ (dashed lines), for values of β of maximum u wall receptivity (table 2).

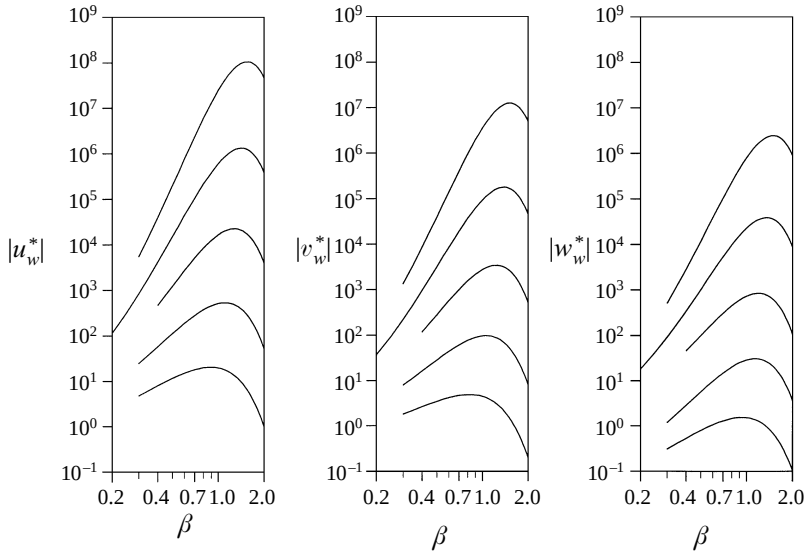

FIGURE 11. Modulus of the (real) wall wavenumber receptivity at $\alpha = 0$ as a function of β. G increases from bottom to top in steps of five starting from $G = 10$ up to $G = 30$.

and u, v and w wall disturbances) and relatively similar, but not identical, regions of maximum receptivity for the different types. Optimal disturbance shapes can be immediately identified as they are proportional to the receptivity itself.

Wavenumber receptivities are readily obtained as Fourier transforms. They, too, exhibit a rather smooth behaviour, the most striking feature being perhaps that both

free-stream and wall-disturbance receptivities peak at zero (respectively, wall-normal and streamwise) wavelength The transfer-function plots of figures 7 and 11 exhibit the general appearance of a single-pole low-pass filter.

The need to adopt different receptivity curves at different Görtler numbers stems from the fact that, owing to boundary-layer growth, the region of maximum amplification shifts to larger and larger (non-dimensional) β with increasing x, and although receptivity takes place in the initial portion of the boundary layer, it takes place differently at different wavenumbers.

As far as the overall energetic yield is concerned, the relative effectiveness of different generation mechanisms is strongly affected by the different scaling of longitudinal and crossflow velocity components in the boundary layer. In fact, whereas the effectiveness of longitudinal-velocity (streak) disturbances can be assessed directly from the figures given above and is a function of the Görtler number alone, in the case of crossflow initial or wall disturbances the ratio between final longitudinal and initial transverse kinetic energy must eventually be multiplied by the Reynolds number in order that the two energies be measured in the same units. It is clear that, independently of any amplification provided by the Görtler mechanism, an energetic ratio as high as desired can always be obtained for crossflow (roll) disturbances by increasing the Reynolds number enough. This behaviour ensues from the persistence of an instability even in the absence of any curvature (Luchini 1996).

It goes without saying that the mathematical possibility of calculating a Green's function from the solution of the adjoint of an evolution problem has been known for quite a long time; in particular, it has been developed to a high level of refinement in the discipline known as Optimal Control. Optimal control of systems governed by ordinary differential equations is more or less a textbook topic, and the mathematical properties of optimal control as applied to partial differential equations have also been thoroughly scrutinized (Lions 1968). Nevertheless, the potential of this method for the understanding of fluid-dynamic instabilities is just beginning to be exploited. The only other examples we know of are Farrell & Moore (1992) who developed a theory of optimal – non-exponentially growing – perturbations in oceanographic flows, and Hill (1992) who worked on the restabilization of laminar cylinder wakes (both works were brought to our attention during the refereeing phase of the present paper); even more recently, Hill (1995, 1996) and Herbert (1997) gave results on the receptivity of some boundary-layer instabilities, in particular through the solution of the adjoint form of the so-called Parabolized Stability Equations (see Bertolotti, Herbert & Spalart 1992 for a thorough discussion of the properties of the PSE).

It is clear that the present type of 'reverse' approach is not limited to the Görtler problem; quantitative receptivity calculations for other classical types of instability can and will be performed in the next few years. Given its connection with optimal control, this reverse method of receptivity calculation is also ideally suited for problems of flow control and transition delay. It does not seem difficult, in fact, to devise a strategy of wall and/or inflow forcing in such a way as to minimize the amplitude of the downstream instability mode.

Some of the results described in this paper were reported at the Sixth European Turbulence Conference – ETC-VI (Lausanne, Switzerland, 2–5 July 1996) and at the DFD Meeting of the American Physical Society (Syracuse, NY, USA, 23–26 November 1996). P. L. has been supported by the Swiss Leonhard Euler Center for Fluid Mechanics, through several grants for extended visits at the EPFL, and by the Italian Ministry of University and Research. A. B. acknowledges support of the Swiss

National Fund, grant no. 2118-036035.92. We thank Peter Corbett for bringing the paper by Farrell & Moore (1992) to our attention.

REFERENCES

Bassom, A. P. & Hall, P. 1994 On the receptivity problem for $O(1)$ wavelength Görtler vortices. *Proc. R. Soc. Lond.* A **446**, 499.

Bassom, A. P. & Seddougui, S. O. 1995 Receptivity mechanisms for Görtler vortex modes. *Theor. Comput. Fluid Dyn.* **7**, 317.

Bertolotti, F. P. 1993 Vortex generation and wave-vortex interaction over a concave plate with roughness and suction. *ICASE Rep.* 93-101.

Bertolotti, F. P., Herbert, T. & Spalart, P. R. 1992 Linear and nonlinear stability of the Blasius boundary layer. *J. Fluid Mech.* **242**, 441.

Bottaro, A., Klingmann, B. G. B. & Zebib, A. 1996 Görtler vortices with system rotation. *Theor. Comp. Fluid Dyn.* **8**, 325.

Bottaro, A. & Luchini, P. 1996 The linear stability of Görtler vortices revisited. In *Mathematical Modeling and Simulation in Hydrodynamic Stability* (ed. D. N. Riahi), p. 1. World Scientific.

Bottaro, A. & Luchini, P. 1998 Görtler vortices: Are they amenable to local eigenvalue analysis? *Eur. J. Mech.* Submitted for publication.

Bottaro, A. & Zebib, A. 1997 Görtler vortices promoted by wall roughness. *Fluid Dyn. Res.* **19**, 343.

Butler, K. M. & Farrel, B. F. 1992 Three-dimensional optimal perturbations in viscous shear flow. *Phys. Fluids* A **4**, 1637.

Carrier, G. F. 1946 The boundary layer in a corner. *Q. Appl. Maths* **4**, 367.

Denier, J. P., Hall, P. & Seddougui, S. O. 1991 On the receptivity problem for Görtler vortices: vortex motions induced by wall roughness. *Phil. Trans. R. Soc. Lond.* A **335**, 51.

Farrell, B. F. & Moore, A. M. 1992 An adjoint method for obtaining the most rapidly growing perturbation to oceanic flows. *J. Phys. Oceanogr.* **22**, 338.

Floryan, J. M. & Saric, W. S. 1979 Stability of Görtler vortices in boundary layers with suction. *AIAA Paper* 79-1497.

Floryan, J. M. & Saric, W. S. 1982 Stability of Görtler vortices in boundary layers. *AIAA J.* **20**, 316.

Görtler, H. 1941 Instabilität laminarer Grenzschichten an konkaven Wänden gegenüber gewissen dreidimensionalen Störungen. *Z. Angew. Math. Mech.* **21**, 250.

Goulpié, P., Klingmann, B. G. B. & Bottaro, A. 1996 Görtler vortices in boundary layers with streamwise pressure gradient: Linear theory. *Phys. Fluids* **8**, 451.

Hall, P. 1982 Taylor–Görtler vortices in fully developed or boundary-layer flows: linear theory. *J. Fluid Mech.* **124**, 475.

Hall, P. 1983 The linear development of Görtler vortices in growing boundary layers. *J. Fluid Mech.* **130**, 41.

Hall, P. 1990 Görtler vortices in growing boundary-layers: the leading edge receptivity problem, linear growth and the nonlinear breakdown stage. *Mathematika* **37**, 151.

Herbert, T. 1997 Parabolized stability equations. *Ann. Rev. Fluid Mech.* **29**, 245.

Hill, D. C. 1992 A theoretical approach for analyzing the restabilization of wakes. *AIAA Paper* 92-0067.

Hill, D. C. 1995 Adjoint systems and their role in the receptivity problem for boundary layers. *J. Fluid Mech.* **292**, 183.

Hill, D. C. 1996 Receptivity and control in non-parallel flows. *Bull. Am. Phys. Soc.* **41**, 1777.

Kaplun, S. 1954 The role of coordinate systems in boundary-layer theory. *Z. Angew. Math. Phys.* **5**, 111.

Lions, J. L. 1968 *Contrôle Optimal de Systèmes Gouvernés par des Equations aux Derivées Partielles.* Gauthier-Villars, Paris.

Luchini, P. 1996 Reynolds-number-independent instability of the boundary layer on a flat plate. *J. Fluid Mech.* **327**, 101.

Moore, F. K. 1956 Three-dimensional boundary layer theory. *Adv. Appl. Mech.* IV, 159.

PEXIEDER, A. 1996 Effects of system rotation on the centrifugal instability of the boundary layer on a curved wall: An experimental study. PhD Thesis, EPFL, no. 1507.

SARIC, W. S. 1994 Görtler vortices. *Ann. Rev. Fluid Mech.* **26**, 379.

TING, L. 1965 On the initial conditions for boundary layer equations. *J. Math. Phys.* **44**, 353.